Biaxially Self-Reinforced High-Density Polyethylene Prepared by Dynamic Packing Injection Molding. II. Microstructure Investigation

Jun Lei,[1] Chaodong Jiang,[1] Kaizhi Shen[1,2]

[1]*College of Polymer Science and Engineering, Sichuan University, Chengdu, Sichuan 610065, China*
[2]*Key Laboratory of Polymer Engineering, Sichuan University, Chengdu, Sichuan 610065, China*

Received 14 July 2003; accepted 18 February 2004
DOI 10.1002/app.20639
Published online in Wiley InterScience (www.interscience.wiley.com).

ABSTRACT: Differential scanning calorimetry, wide-angle X-ray diffraction, small-angle X-ray scattering, and transmission electron microscope are employed to study the microstructure of biaxially self-reinforced high-density polyethylene (HDPE) prepared in uniaxial oscillating stress field by dynamic packing injection molding. The results indicate that the biaxial self-reinforcement of HDPE is mainly due to the existence of interlocking shish-kebab morphology (i.e., zip fastener structure), along with the orientation of lamellae and molecular chains and the enhanced crystallinity. © 2004 Wiley Periodicals, Inc. J Appl Polym Sci 93: 1591–1596, 2004

Key words: reinforcement; polyethylene (PE); injection molding; microstructure; dynamic packing

INTRODUCTION

The crystal morphology of conventional injection-molded (CIM) high-density polyethylene (HDPE) is mainly spherulitic. Nevertheless, our previous work revealed that the self-reinforced HDPE prepared by dynamic packing injection molding (DPIM) featured orientated shish-kebab morphology.[1–7] Further, Bashir and Odell reported the high-modulus, high-strength splinter-resistant thick HDPE filaments produced in uniaxial flow by capillary extrusion had a specific interlocking shish-kebab morphology. They predicted the existence of this morphology could result in good mechanical properties in both flow direction (MD) and transverse direction (TD).[8] In our preceding article, biaxially self-reinforced HDPE was prepared in uniaxial oscillating flow field supplied by DPIM.[9] Thus, it seems that the formation of the above-mentioned interlocking morphology can account for the effect of biaxial self-reinforcement. Here, this article concentrates on microstructure investigation of biaxially self-reinforced HDPE moldings.

Correspondence to: K. Shen (leijun10@263.net).
Contract grant sponsor: National Natural Science Foundation of China; contract grant number: 29574168.
Contract grant sponsor: Doctor Foundation of China; contract grant number: 2000061021.

EXPERIMENTAL

Material

The material used in this work was HDPE (7006A, Qilu Petrochemical Corp., Shandong, China) with a melt index of 6.8 g/10 min (ASTM D1238).

Preparation of injection moldings

The injection moldings were prepared by DPIM and static packing injection molding (SPIM) under the processing parameters described in detail in our preceding article.

Differential scanning calorimetry (DSC)

DSC measurements were performed with slices (about 0.5 mm thick) taken parallel to the flow direction from the specimens prepared by static and dynamic packing injection molding on Perkin–Elmer DSC-2. The slices were cut at varying distances from the surfaces. The heating rate was 10°C/min.

Wide-angle X-ray diffraction (WAXD)

CuK_α radiation was used for X-ray diffractometry. The $10 \times 10 \times 1$ mm slice samples were cut from the surface and the core region of the static and dynamic injection moldings, respectively, parallel to

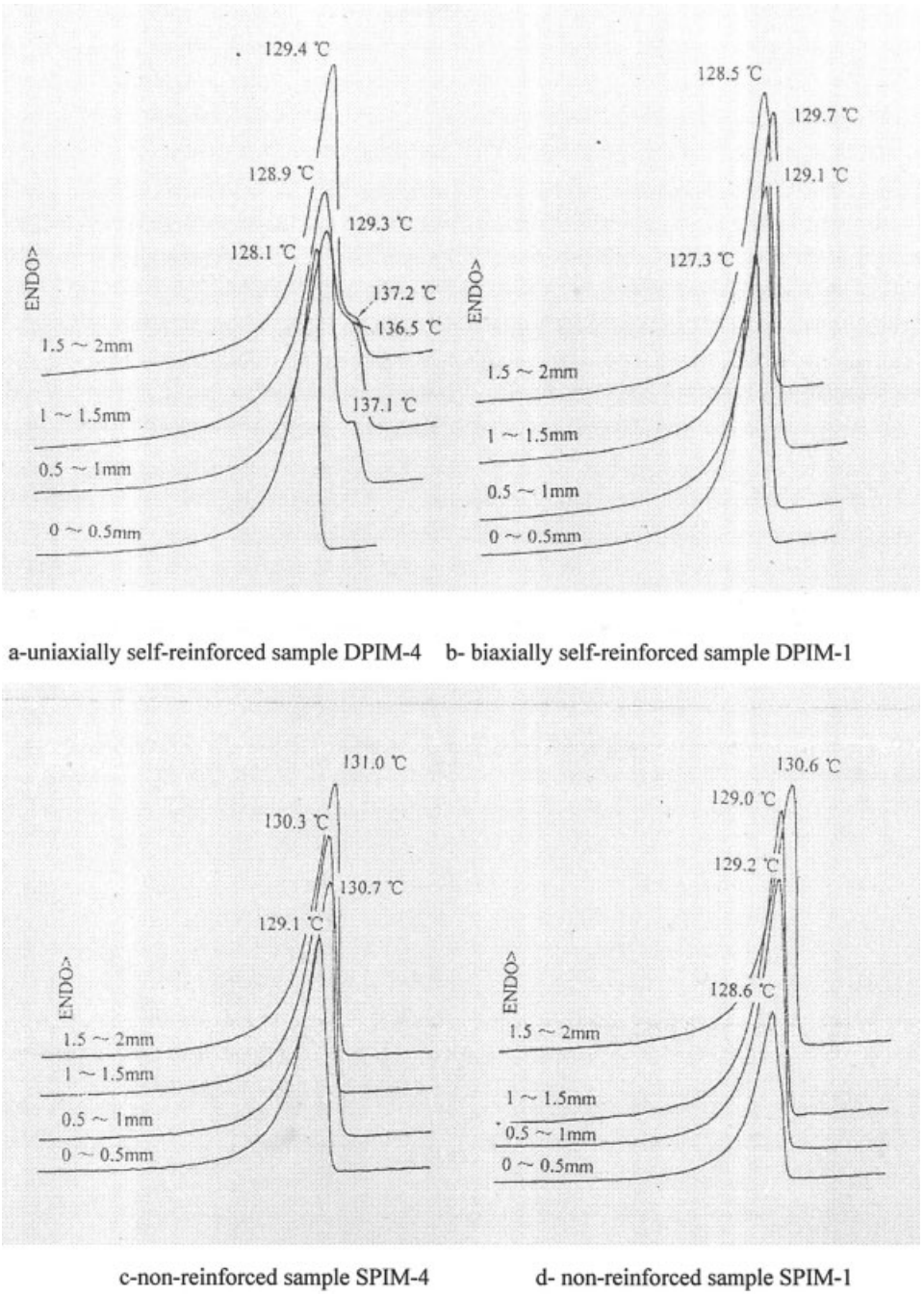

Figure 1 DSC curves of different layers in samples. (a) Uniaxially self-reinforced sample DPIM-4; (b) Biaxially self-reinforced sample DPIM-1; (c) non-reinforced samples SPIM-4; (d) non-reinforced sample SPIM-1.

the MD. A × D/MAX-A diffractometer was used to record diffraction profiles when scanning at a rate of 0.6° 2θ /s over an angular range $0° \leq 2\theta \leq 45°$.

Small-angle X-ray scattering (SAXS)

Ni-filtered CuK_α radiation was used for X-ray scattering. The 30 × 10 × 2 mm slice samples were cut from the surface and the core of the static and dynamic injection moldings, respectively, parallel to the injection direction. A 3015 X-ray scatterometer was employed in the SAXS measurement.

Transmission electron microscope (TEM)

The central layers of DPIM-2, DPIM-4, and SPIM-2 were frozen in liquid nitrogen, sliced parallel to MD,

TABLE I
DSC Test Results of DPIM Samples

	DPIM-4				DPIM-1			
Depth of slice	0–0.5 mm	0.5–1.0 mm	1.0–1.5 mm	1.5–2.0 mm	0–0.5 mm	0.5–1.0 mm	1.0–1.5 mm	1.5–2.0 mm
Melt point (°C)	128.1	129.3	128.9	129.4	127.3	129.1	129.7	128.5
Melt range (°C)	37.0	39.2	41.3	39.1	36.3	35.8	36.4	34.8
Melt enthalpy (Cal/g)	41.25	46.67	47.39	46.47	40.60	45.20	44.87	44.53
Crystallinity (%)	60.3	68.2	69.3	67.9	59.4	66.1	65.6	65.1

and stained with ruthenium tetraoxide (RuO_4).[10] Then, the morphologies of these superthin slices were observed on a Hitachi H-800 SE microscope.

RESULTS AND DISCUSSION

DSC results

Figure 1(a–d) shows the DSC curves of slices in various depths of uniaxially self-reinforced samples (DPIM-4), biaxially self-reinforced samples (DPIM-1), and two non-reinforced samples (SPIM-4 and SPIM-1), respectively. SPIM-4 and SPIM-1 were used for comparison purposes. The results are shown in Tables I and II, respectively.

It is shown in Figure 1, Table I, and Table II that both biaxially and uniaxially self-reinforced samples have a much wider melting range than non-reinforced samples. This indicates the formation of multiple crystalline morphologies or lamellae with different thicknesses. Uniaxially self-reinforced DPIM-4 samples have not only lower melting peak, but also exhibit a shoulder at higher temperature (137°C). Lower temperature melting peak is due to the melting of spherulites and overgrown lamellae in shish-kebab crystals, which exhibit lower thermal stability, while higher temperature melting peak is produced by the melting of extended-chain crystal cores that are more stable.[3] The biaxially self-reinforced sample DPIM-1 just exhibits only one lower temperature main peak resulted from the melting of the lamellar outgrowths. The only melting peak of biaxially self-reinforced DPIM-1 samples means that the shish-kebab crystals in DPIM-1 have an extremely low proportion of central extended-chain filaments and are mainly composed of lamellae (refer to TEM results discussed later).

The crystallinity of each slice was calculated on the basis of following relationship of melt enthalpy and crystallinity of polymer

$$\alpha_c = \frac{\Delta H_f}{\Delta H_{f\alpha}} \times 100\% \quad (1)$$

where α_c is crystallinity, and ΔH_f stands for melt enthalpy, and $\Delta H_{f\alpha}$ represents the melt enthalpy of the same polymer with 100% crystallinity (e.g., 68.4 Cal/g for HDPE).

According to the calculated crystallinity listed in Tables I and II, the crystallinity of each DPIM sample is higher than that of its comparative SPIM sample. This is due to the existence of higher elongational and shearing flow in DPIM, which is beneficial to crystallization of melt. Moreover, the crystallinities of DPIM-4 and SPIM-4 are higher than those of DPIM-1 and SPIM-1, respectively. This can be attributed to the difference of processing parameters between comparative samples. Compared to that of DPIM-1 and SPIM-1, the higher packing pressure of DPIM-4 and SPIM-4 results in higher strain rates in processing, which is favorable to the growth of crystals.

WAXD results

Figure 2 exhibits the WAXD profiles of uniaxially self-reinforced sample DPIM-4, biaxially self-reinforced sample DPIM-1, and non-reinforced sample SPIM-1. Figure 2(a) is for skin region and Figure 2(b)

TABLE II
DSC Test Results of SPIM

	SPIM-4				SPIM-1			
Depth of slice	0–0.5 mm	0.5–1.0 mm	1.0–1.5 mm	1.5–2.0 mm	0–0.5 mm	0.5–1.0 mm	1.0–1.5 mm	1.5–2.0 mm
Melt point (°C)	129.1	130.7	130.3	131.0	128.6	129.2	129.0	130.6
Melt range (°C)	28.3	31.3	28.9	30.7	28.4	29.5	28.4	28.4
Melt enthalpy (Cal/g)	40.05	42.91	43.99	44.30	38.95	42.07	42.87	42.85
Crystallinity (%)	58.6	62.7	64.3	64.7	56.9	61.5	62.7	62.6

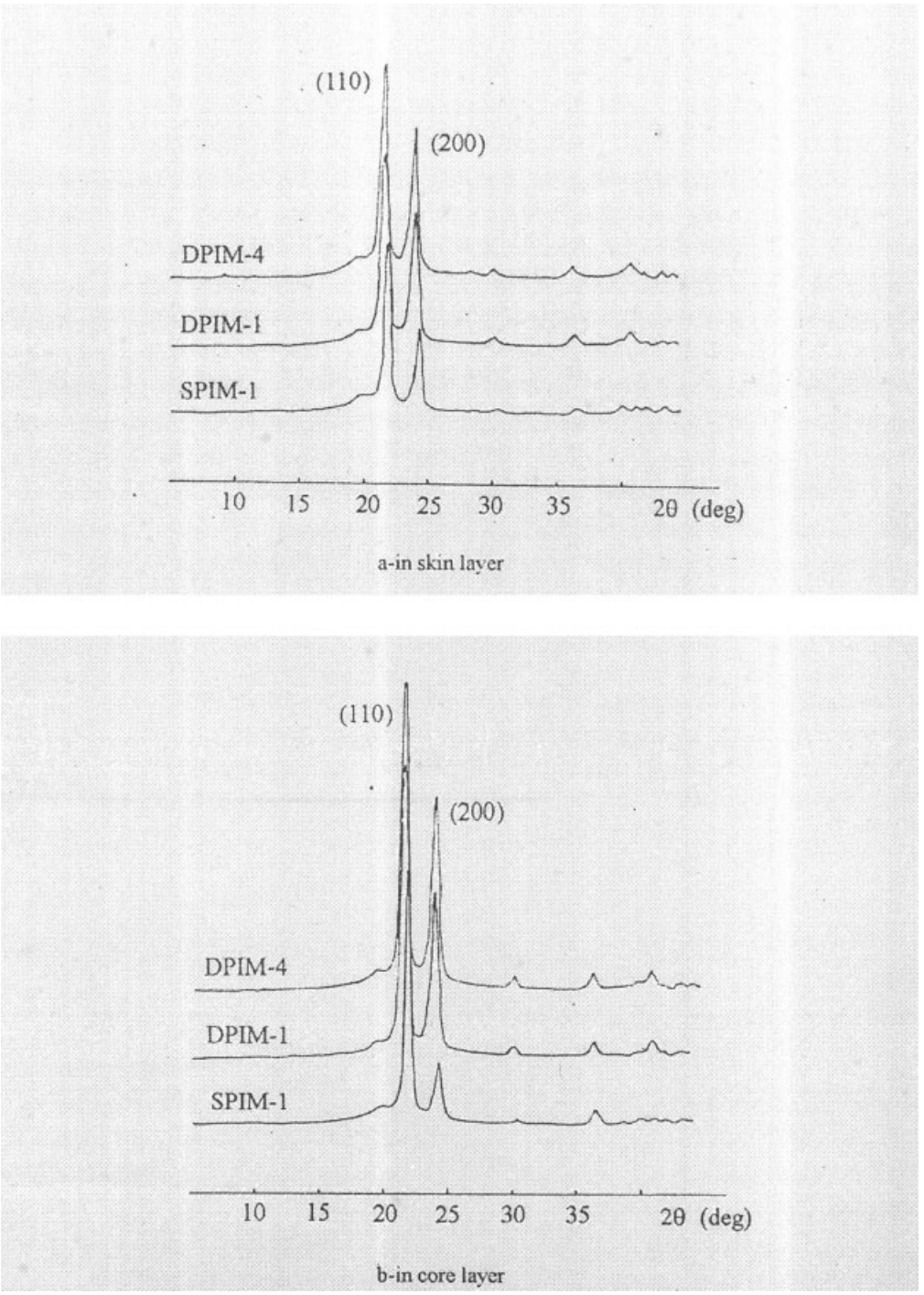

Figure 2 Comparison of WAXD profiles of uniaxially self-reinforced sample DPIM-4, biaxially self-reinforced sample DPIM-1, and non-reinforced sample SPIM-1.

is for core region. The calculated results are listed in Table III.[11]

Figure 2 (a, b) suggests that the intensities of the crystalline planes (110) and (200) of self-reinforced samples DPIM-4 and DPIM-1 have greatly increased. This indicates that the crystal planes of self-reinforced moldings have oriented. Another fact is that the intensity of each plane of uniaxially self-reinforced sample DPIM-4 is slightly higher than that of biaxially self-reinforced sample DPIM-1. This is decided by the different processing parameters between the DPIM-4 and DPIM-1. DPIM-4 had higher packing pressure and, therefore, higher strain rate than DPIM-1, causing a high degree of orientation. For the same self-reinforced molding, the orientation degree of the core layer was higher than that of the skin layer, because of

TABLE III
Unicell Parameters, Crystallite Size, and Crystallinity Calculated by WAXD Results

Samples	a	b	$H_{(110)}$	$H_{(200)}$	α_c
DPIM-4 surface	7.458	4.969	101.85	102.27	69.29
DPIM-4 core	7.450	4.969	101.85	102.27	69.17
DPIM-1 surface	7.440	4.960	101.85	95.98	63.47
DPIM-1 core	7.430	4.949	101.86	102.29	68.47
SPIM-1 surface	7.356	4.889	101.90	109.43	50.00
SPIM-1 core	7.382	4.908	108.96	109.58	52.41

Note. a, b, unicell parameters (Å); H, crystallite size (Å); α_c, crystallinity (%).

the same reason. Although the same rule is applicable to the same non-reinforced molding SPIM-1, the reason is that the melt in skin region had a low temperature and froze quickly before orientation.

In Table III, the unicell parameters and the crystallite size of self-reinforced samples and non-reinforced samples hold consistent with each other within the experimental error. It indicates that they have nearly the same unicell structure and crystal form. Additionally, the crystallinities of uniaxially self-reinforced samples, biaxially self-reinforced samples, and non-reinforced samples decrease in turn, which is also related to the variation in strain rate resulted from various packing pressures in processing.

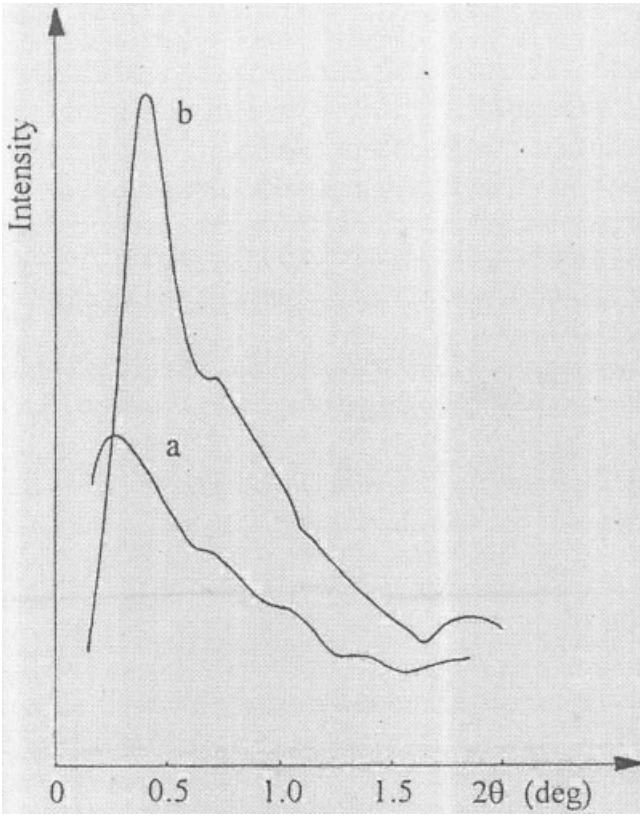

Figure 3 Comparison of SAXS profiles of biaxially self-reinforced sample DPIM-2 (a) and non-reinforced sample SPIM-2 (b).

TABLE IV
SAXS Results

Samples	SPIM-2	DPIM-2
Long period (Å)	248	417
Crystalline thickness (Å)	141	188
Amorphous thickness (Å)	107	229
Uniaxial crystallinity (%)	57	45

SAXS results

Figure 3 shows the SAXS profiles after Lorentz's modification. It is very clear that the biaxially self-reinforced DPIM-2 sample has much lower and more uniform scattering intensity than the non-reinforced SPIM-2 sample does. This indicates that the orientation degree of amorphous phase in self-reinforced molding is increased considerably, and then, the density difference of electron cloud between the crystalline phase and the amorphous phase is decreased substantially.

From the SAXS measurement results shown in Table IV, it can be seen that self-reinforced sample DPIM-2 has a much higher long period, thickness of crystalline region, and amorphous region than the non-reinforced sample SPIM-2 does. The reason is that the higher strain field of dynamic packing extends the molecular chains in both the crystalline and the amorphous regions more efficiently and the thicknesses of the two regions are increased.

The crystallinity of DPIM-2 is lower than that of SPIM-2. It is noticeable and contradictory to the DSC test results. In fact, the calculation of crystallinity from SAXS results is based on a two-phase model, which regards the transitional phase between crystalline and amorphous phases as amorphous, and therefore, the crystallinity of DPIM-2 is lower.

TEM results

Figure 4(a–c) shows the TEM micrographs of biaxially self-reinforced sample DPIM-2, uniaxially self-reinforced sample DPIM-4, and non-reinforced sample SPIM-2, respectively. The bright areas stand for crystalline phases, and the dark areas belong to amorphous phases. Figure 5(a) shows that the crystalline phase of biaxially self-reinforced sample DPIM-2 really features an interlocking shish-kebab morphology. The horizontally grown lamellae are stacked up into three columns along the MD. For each column, the aligned normal of lamellae implies the existence of a central filament with a length of 3–4 μm, and the lamellae grow perpendicular to central filament with

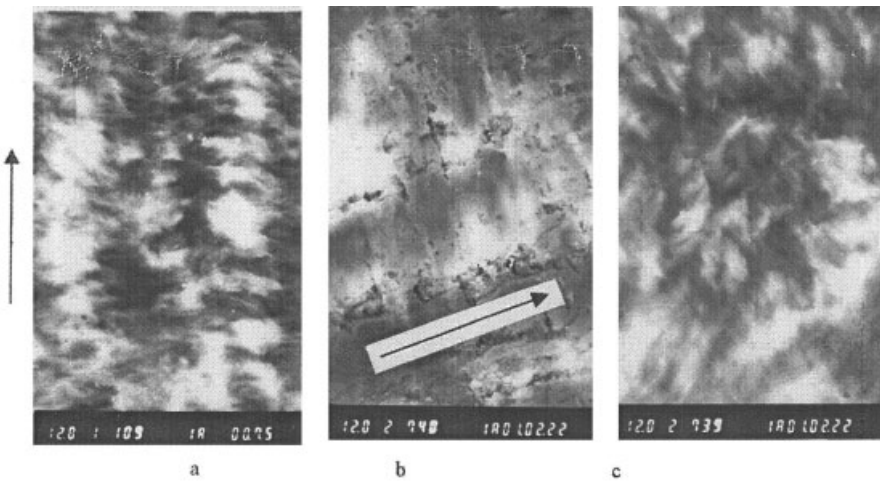

Figure 4 (a) Transmission electron micrographs of biaxially self-reinforced sample DPIM-2, (b) uniaxially self-reinforced sample DPIM-4, and (c) non-reinforced sample SPIM-2. (The arrows indicate the shearing directions and the magnification is ×12,000.)

an approximate width of 1 μm. The wedges of lamellae belong to different shish-kebab overlap and lock each other. Referring to the model of interlocking shish-kebab structure proposed by Odell et al.,[8,12] we can regard the morphology as an interlocking shish-kebab structure. Obviously, the enhancement of tensile strengths in both MD and TD are mainly resulted from this structure.[13,14] Here, we substantiate the prediction of Odell et al. that a wide sheet-formed specimen with such morphology would have good mechanical properties in both MD and TD.[8] In Figure 5(b), uniaxially self-reinforced sample DPIM-4 has thicker central filaments, and this explains the existence of the higher temperature melting peaks in its DSC curve. Apparently, the higher orientation degree of central filament and lamellae coincides with the WAXD results. The thicker and higher orientated filaments account for the highly improved tensile strength in MD but weakened tensile strength in TD. It is evident from Figure 5(c) that the crystals in non-reinforced sample SPIM-2 are mainly lower oriented lamellae. This explains its lower mechanical properties in both MD and TD.

CONCLUSION

Microstructure studies show that the self-reinforced HDPE prepared by DPIM has higher crystallinity, higher orientation degree in both crystalline and amorphous phases, and well-oriented shish-kebab morphology. More specifically, the biaxially self-reinforced HDPE has the interlocking shish-kebab morphology as its characteristic structure. The effect of biaxial self-reinforcement achieved in a uniaxial oscillating stress field is attributed to the formation of such a special morphology.

The authors gratefully acknowledge the financial support from the National Natural Science Foundation of China (29574168) and the Doctor Foundation of China (2000061021).

References

1. Guan, Q.; Shen, K. Z.; Ji, J. L. J Appl Polym Sci 1995, 55, 1797.
2. Guan, Q.; Shen, K. Z. Chem J Chin Univ, 1995, 16, 1129.
3. Guan, Q.; Lai, F. S.; McCarthy, S. P. Polymer 1997, 38, 5251.
4. Kalay, G.; Kalay, C. R. J Polym Sci, Part B: Polym Phys 2002, 40, 1828.
5. Kalay, G.; Kalay, C. R. J Appl Polym Sci 2003, 88, 3, 814.
6. Zhang, G.; Fu, Q.; Shen, K. Z.; Jiang, L.; Wang. Y. J Appl Polym Sci 2002, 86(1), 58.
7. Na, B.; Zhang, Q.; Fu, Q.; Zhang, G.; Shen, K. Z. Polymer 2002, 43, 7367.
8. Bashir Z., Odell J. A., J Mater Sci 1993, 28, 1081.
9. Lei, J.; Jiang, C.; Shen K. J Appl Polym Sci, to appear.
10. Chen, S. X.; Jin, Y. Z. Trans Electron Micros 1992, 3, 206.
11. Wu, R. J. Modern Measurements Applied to Polymer; Press of Shanghai Sci. Tech: Shanghai, 1986; pp 335–340.
12. Odell J. A., Grubb D. T., Keller A., Polymer 1978, 19, 617.
13. Chen, L. -M.; Shen, K. Z. J Appl Polym Sci 2000, 78, 1906.
14. Chen, L. -M.; Shen, K. Z. J Appl Polym Sci 2000, 78, 1911.